RAA 2021 Vol. **21** No. **10**, 254(8pp) doi: 10.1088/1674-4527/21/10/254

http://www.raa-journal.org *http://iopscience.iop.org/raa*

Research in Astronomy and Astrophysics

The isotropic energy function and formation rate of short gamma-ray bursts

Zhi-Ying Liu[1], Fu-Wen Zhang[1,2] and Si-Yuan Zhu[1]

[1] College of Science, Guilin University of Technology, Guilin 541004, China; *fwzhang@pmo.ac.cn*

[2] Key Laboratory of Dark Matter and Space Astronomy, Chinese Academy of Sciences, Nanjing 210008, China

Received 2021 February 10; accepted 2021 June 29

Abstract Gamma-ray bursts (GRBs) are brief, intense, gamma-ray flashes in the universe, lasting from a few milliseconds to a few thousand seconds. For short gamma-ray bursts (sGRBs) with duration less than 2 seconds, the isotropic energy ($E_{\rm iso}$) function may be more scientifically meaningful and accurately measured than the luminosity ($L_{\rm p}$) function. In this work we construct, for the first time, the isotropic energy function of sGRBs and estimate their formation rate. First, we derive the $L_{\rm p} - E_{\rm p}$ correlation using 22 sGRBs with known redshifts and well-measured spectra and estimate the pseduo redshifts of 334 Fermi sGRBs. Then, we adopt the Lynden-Bell c^- method to study isotropic energy functions and formation rate of sGRBs without any assumption. A strong evolution of isotropic energy $E_{\rm iso} \propto (1+z)^{5.79}$ is found, which is comparable to that between $L_{\rm p}$ and z. After removing effect of the cosmic evolution, the isotropic energy function can be reasonably fitted by a broken power law, which is $\phi(E_{\rm iso,0}) \propto E_{\rm iso,0}^{-0.45}$ for dim sGRBs and $\phi(E_{\rm iso,0}) \propto E_{\rm iso,0}^{-1.11}$ for bright sGRBs, with the break energy 4.92×10^{49} erg. We obtain the local formation rate of sGRBs is about 17.43 events $\rm Gpc^{-3}\ yr^{-1}$. If assuming a beaming angle is 6° to 26°, the local formation rate including off-axis sGRBs is estimated as $\rho_{0,\rm all} = 155.79 - 3202.35$ events $\rm Gpc^{-3}\ yr^{-1}$.

Key words: gamma-ray bursts: general — methods: data analysis

1 INTRODUCTION

Gamma-ray bursts (GRBs) are the most dramatic explosions in the universe (see e.g., Piran 2004; Mészáros 2006; Zhang 2007). These events are so bright that they can be observed at higher redshifts than supernovae (SNe), which are powerful tools for exploring the early universe (see e.g., Ghirlanda et al. 2006; Zhang 2011; Wang et al. 2015). Traditionally, GRBs can be divided into two groups, long GRBs (lGRBs) and short GRBs (sGRBs), based on the well-known bimodal nature of the duration distribution with a separation at about $T_{90} \sim$ 2s (Kouveliotou et al. 1993). It is generally believed that some lGRBs are associated with the deaths of massive stars (also called collapsars), while some sGRBs are produced by the merging of the binary compact objects (see e.g., Eichler et al. 1989; Narayan et al. 1992; Lipunov et al. 1995) such as neutron star-neutron star (NS-NS) and neutron star-black hole (NS-BH). The detection of gravitational wave event GW 170817 associated with GRB 170817A, has confirmed that at least a fraction of the observed sGRBs are produced by the merger of binary neutron stars (Abbott et al. 2017).

The luminosity function and the formation rate $\rho(z)$ is crucial to understand the nature of GRBs (Pescalli et al. 2016). With the number of GRBs with known redshifts is increasing, the lGRB luminosity function and formation rate have been widely explored (see e.g., Yonetoku et al. 2004; Salvaterra et al. 2009; Wanderman & Piran 2010; Salvaterra et al. 2012; Wang et al. 2013; Yu et al. 2015; Pescalli et al. 2016; Lan et al. 2019). However, only a small fraction of sGRBs have redshift measurements, therefore the sGRB formation rate is very difficult to estimate. Recently, using the empirical correlations, some authors tentatively have estimated the pseudo redshifts and have derived the luminosity function and formation rate of sGRBs. Yonetoku et al. (2014) determined the redshifts of 72 BATSE sGRBs without a known redshift using the $L_{\rm p} - E_{\rm p}$ correlation between the peak luminosity $L_{\rm p}$ and the rest frame peak energy $E_{\rm p}$, and found that the formation rate of sGRBs at $z = 0$ is 0.63 events $\rm Gpc^{-3} yr^{-1}$. Using the same $L_{\rm p} - E_{\rm p}$ correlation, Zhang et al. (2018) derived the pseudo redshifts of 284 Fermi sGRBs and studied the luminosity function and formation rate of sGRBs. They found that the formation rate decreases rapidly at $z < 1.0$ and the local formation rate is 7.53 events $\rm Gpc^{-3}\ yr^{-1}$. Guo et al. (2020) discovered a universal three parameter correlation among $L_{\rm p}$, $E_{\rm p}$ and the "high signal" timescale $T_{0.45}$ for both long and short GRBs, which can be used a redshift estimator, and they also determined the luminosity function and formation rate of sGRBs using the Swift sample and found that the local formation rate is 15.5 events $\mathrm{Gpc}^{-3}\,\mathrm{yr}^{-1}$.

However, the durations of most of sGRBs are very short, and even only a few milliseconds. We know that the luminosity function was originally used to study long-lasting and relatively stable astrophysical phenomena, such as stars and galaxies, the isotropic energy ($E_{\rm iso}$) function probably provides an independent or even more representative clue to the underlying physics as shown in Wu et al. (2012). Thus, in this work we focus on the isotropic energy function rather than on the traditional luminosity function.

In this paper, we study the isotropic energy function and the formation rate of Fermi sGRBs. This paper is organized as follows. In Section 2, we introduce our sample and data selection, then we derive the $L_{\rm p} - E_{\rm p}$ correlation and the pseudo redshifts of sGRBs detected by the Fermi detector. In Section 3, the isotropic energy function and formation rate of sGRBs are obtained using the Lynden-Bell c^{-} method. Finally, we give conclusions and discussion in Section 4. Throughout this paper, we adopt the standard float cold dark matter cosmology with the typical cosmological parameters $\Omega_{\rm m} = 0.27$ and $H_0 = 70\ \mathrm{km\,s^{-1}\,Mpc^{-1}}$.

2 SGRB SAMPLE AND DATA ANALYSIS

We concentrate our analysis on the sGRBs detected only by the Fermi detector to minimize the influence of different instruments (with different sensitivities and energy bands). The Fermi GRBs are selected from the Fermi catalog[1] until the end of January 2020, in total, there are 2698 events. First, according to the traditional sGRB definition method ($T_{90} < 2\,\mathrm{s}$), we select the bursts with well-measured spectral parameters and duration less than 2 s, in total there are 367 events.

To obtain a more precise and robust result of the isotropic energy function and formation rate for sGRBs, a large number of sGRBs with known redshifts are needed. Although the number of the Fermi sGRBs is sufficient to make a statistical analysis, the bursts with measured redshift are indeed quite limited, we need to expand the redshift sample. Previous authors have been estimated the pseudo redshifts of sGRBs using the $L_{\rm p} - E_{\rm p}$ correlations (see e.g., Yonetoku et al. 2014; Zhang et al. 2018). We also use this method to estimate the pseudo redshifts of Fermi sGRBs with unknown redshifts.

We collect 23 sGRBs with known redshifts and measured spectra. In Table 1, we list the properties of these sGRBs, including name, redshift z, the observer frame duration T_{90}, low-energy spectral index α, high-energy spectral index β, peak energy of the νF_ν spectrum in the observer frame $E_{\rm p}^{\rm obs}$, peak flux in a certain energy range $F_{\rm p}$, energy range ($e_{\rm min}$,$e_{\rm max}$), and peak luminosity $L_{\rm p}$. These sGRB spectra were fitted by the best spectral model, and the spectrum is a cut-off power-law (CPL) spectrum if only the low energy photon index α is reported (Sakamoto et al. 2008) or a band function (Band et al. 1993) if the high energy photon index β is also given, which are as follows:

$$N(E) = A\left(\frac{E}{100\ \mathrm{keV}}\right)^{\alpha} \exp^{-\frac{(2+\alpha)E}{E_p}}\,, \tag{1}$$

and

$$N(E) = \begin{cases} A\left(\frac{E}{100\ \mathrm{keV}}\right)^{\alpha} \exp\left(-\frac{E}{E_0}\right) \\ A\left(\frac{E}{100\ \mathrm{keV}}\right)^{\beta} \left[\frac{(\alpha-\beta)E_0}{100\ \mathrm{keV}}\right]^{\alpha-\beta} \exp\left(\beta-\alpha\right) \end{cases}. \tag{2}$$

In this paper, both $E_{\rm iso}$ and $L_{\rm p}$ are corrected to the rest frame energy band of $1 - 10^4$ keV. The peak luminosity is estimated to be

$$L_{\rm p} = 4\pi D_L^2(z) F_{\rm p} k_{\rm c}\,, \tag{3}$$

where $k_{\rm c}$ is the factor of the k-correction, $F_{\rm p}$ is the peak flux in a certain energy range ($e_{\rm min}$, $e_{\rm max}$) and D_L is luminosity distance. If the peak flux $F_{\rm p}$ is in units of $\mathrm{erg\ cm^{-2}\ s^{-1}}$, the parameter of k-correction is defined as

$$k_c = \frac{\int_{1\mathrm{keV}/(1+z)}^{10^4\mathrm{keV}/(1+z)} EN(E)dE}{\int_{e_{\rm min}}^{e_{\rm max}} EN(E)dE}\,. \tag{4}$$

If the peak flux $F_{\rm p}$ is in units of $\mathrm{photons\ cm^{-2}\ s^{-1}}$, the parameter of k-correction is defined as

$$k_c = \frac{\int_{1\mathrm{keV}/(1+z)}^{10^4\mathrm{keV}/(1+z)} EN(E)dE}{\int_{e_{\rm min}}^{e_{\rm max}} N(E)dE}\,, \tag{5}$$

where $N(E)$ is the spectral model of GRBs.

We fit the $L_{\rm p} - E_{\rm p}$ correlation with the simple linear form, the best fit to the correlation is given by $L_{\rm p}/10^{51} = a(E_{\rm p}/keV)^b$, with $a = -4.91 \pm 0.89$, $b = 1.90 \pm 0.31$ and the correlation coefficient is $r = 0.81$. Figure 1 shows the $L_{\rm p} - E_{\rm p}$ correlation, and the solid blue line indicates the best fit. It is worth noting that GRB 170817A, the first short burst associated with a detected gravitational wave signal, is a off-axis event (Abbott et al. 2017; Goldstein et al. 2017), which significantly deviates from the $L_{\rm p} - E_{\rm p}$ correlation and is not included in this fitting. We can rewrite the equation as

$$\frac{D_L^2(z)}{(1+z)^{1.90}} = \frac{10^{46.09}}{4\pi F_{\rm p}}\left(\frac{E_{\rm p}}{\mathrm{keV}}\right)^{1.90}. \tag{6}$$

[1] *https://heasarc.gsfc.nasa.gov/W3Browse/fermi/fermigbrst.html*

Table 1 sGRB Sample with Known Redshifts

GRB	z	T_{90}^{0bs} (s)	α	β	$E_{\rm peak}^{\rm obs}$ (keV)	$F_{\rm p}$ (10^{-6} erg cm^{-2} s^{-1})	$e_{\rm min}$ (keV)	$e_{\rm max}$ (keV)	$L_{\rm p}$ (10^{51} erg s^{-1})
170817A	0.0093	2.05±0.47	$0.14^{+0.59}_{-0.59}$	−−	$215.09^{+54.22}_{-54.22}$	0.14±0.03	10	1000	0.00027±0.0.00006
170428A	0.454	0.140	$-0.47^{+0.28}_{-0.21}$	$-2.46^{+0.52}_{-7.54}$	$982.00^{+394.00}_{-355.00}$	50.00±15.20	20	10000	45.49±13.92
160821B	0.16	1.088±0.977	$-1.40^{+0.25}_{-0.25}$	−−	$91.97^{+27.87}_{-27.87}$	9.51±2.13	10	1000	0.81±0.18
160624A	0.483	0.384±0.405	$-0.62^{+0.21}_{-0.21}$	−−	$1153.31^{+488.47}_{-488.47}$	2.95±0.48	10	1000	4.85±0.79
160410A	1.717	1.588±0.121	$-0.71^{+0.26}_{-0.2}$	−−	$1418.00^{+526.00}_{-358.00}$	6.80±1.70	10	10000	142.44±35.61
150424A	0.3	0.276±0.015	$-0.37^{+0.06}_{-0.05}$	−−	$916.00^{+49.00}_{-47.00}$	17.85±0.86	10	10000	5.23±0.25
150101B	0.134	0.080±0.928	$-1.36^{+0.35}_{-0.35}$	−−	$125.11^{+48.57}_{-48.57}$	0.37±0.06	10	1000	0.020±0.003
131004A	0.717	1.152±0.590	$-1.36^{+0.17}_{-0.17}$	−−	$117.91^{+24.21}_{-24.21}$	0.84±0.23	10	1000	2.33±0.63
130603B	0.3564	0.070±0.009	$-0.67^{+0.10}_{-0.10}$	−−	$607.00^{+61.00}_{-52.00}$	5.81±0.43	10	10000	2.55±0.20
111117A	2.211	0.432±0.082	$-0.50^{+0.17}_{-0.17}$	−−	$543.61^{+102.96}_{-102.96}$	2.98±0.42	10	1000	135.32±19.11
101219A	0.718	0.508±0.041	$-0.07^{+0.18}_{-0.16}$	−−	$590.00^{+64.00}_{-56.00}$	4.48±0.45	10	10000	10.66±1.07
100625A	0.452	0.240±0.276	$-0.59^{+0.13}_{-0.13}$	−−	$483.19^{+63.32}_{-63.32}$	5.97±0.79	10	1000	5.17±0.69
100206A	0.4068	0.176±0.072	$-0.40^{+0.13}_{-0.13}$	−−	$531.82^{+71.71}_{-71.71}$	9.92±0.63	10	1000	6.81±0.43
100117A	0.92	0.256±0.834	$-0.10^{+0.26}_{-0.26}$	−−	$325.43^{+51.09}_{-51.09}$	1.73±0.39	10	1000	7.77±1.74
090927	1.37	0.512±0.231	$-0.64^{+0.32}_{-0.32}$	−−	$175.81^{+41.39}_{-41.39}$	0.54±0.11	10	1000	6.58±1.31
090510	0.903	0.960±0.138	$-0.86^{+0.02}_{-0.02}$	−−	$4727.06^{+348.98}_{-348.98}$	18.30±0.78	10	1000	474.99±20.13
080905	0.1218	0.960±0.345	$0.20^{+0.73}_{-0.73}$	−−	$349.71^{+55.27}_{-55.27}$	2.87±0.45	10	1000	0.11±0.02
071227	0.383	0.714±0.059	$-0.95^{+0.33}_{-0.23}$	−−	$632.00^{+571.00}_{-207.00}$	1.25±0.28	10	10000	0.66±0.15
070714B	0.92	1.256±0.171	$0.19^{+1.1}_{-0.57}$	−−	$551.00^{+148.00}_{-112.00}$	2.30±0.50	10	10000	10.13±2.20
061201	0.111	0.580±0.013	$-0.36^{+0.36}_{-0.28}$	−−	$872.00^{+268.00}_{-188.00}$	5.60±1.30	10	10000	0.18±0.04
061006	0.4377	0.376±0.062	$-0.65^{+0.12}_{-0.11}$	−−	$701.00^{+126.00}_{-101.00}$	4.54±0.54	10	10000	3.25±0.39
051221A	0.5465	0.214±0.050	$-1.12^{+0.1}_{-0.09}$	−−	$511.00^{+118.00}_{-81.00}$	4.10±0.61	10	10000	5.13±0.76
050709	0.1606	0.070	$-0.53^{+0.12}_{-0.12}$	−−	$97.40^{+11.60}_{-11.60}$	5.10±0.50	2	400	0.37±0.04

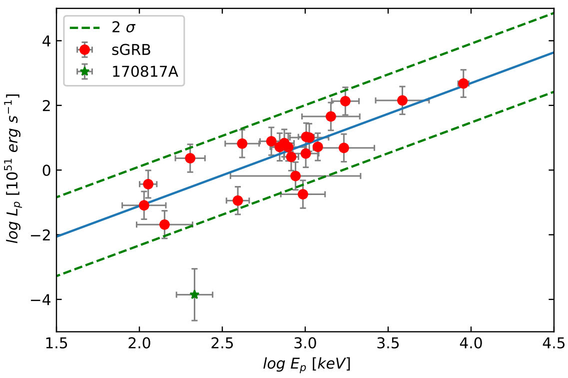

Fig. 1 $L_{\rm p}$ – $E_{\rm p}$ correlation for sGRBs. The *blue line* is the best fit. The *green dotted lines* show the 2σ prediction band.

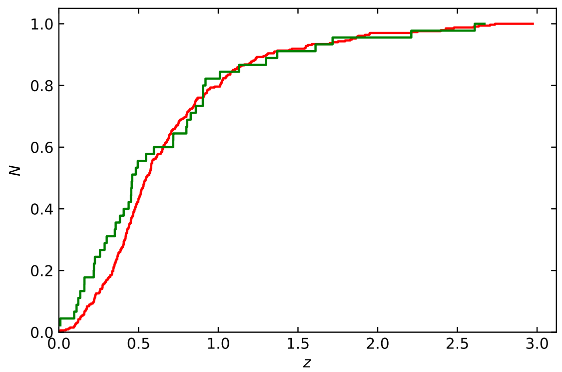

Fig. 2 The cumulative distributions of the pseudo redshifts for Fermi sGRBs and the measured redshifts of sGRBs with well measured spectra. *Solid red line* and *solid green line* represent the pseudo redshifts and the measured redshifts, respectively.

We use Equation (6) to derive pseudo redshifts of 368 Fermi sGRBs. The sGRBs with $z > 3$ are removed from our sample, because the maximum redshift observed for sGRBs is 2.67 so far. Hereafter we use 334 sGRBs to make the further analysis. The results are shown in Table 2. To confirm whether or not our determined redshift is consistent with one of the measured redshifts, we compare the redshift cumulative distributions of observed sGRBs and 334 Fermi sGRBs as shown in Figure 2, where the solid green line represents the cumulative distribution of the measured redshifts of sGRBs and the solid red line represents that of the pseudo redshifts of Fermi sGRBs. We

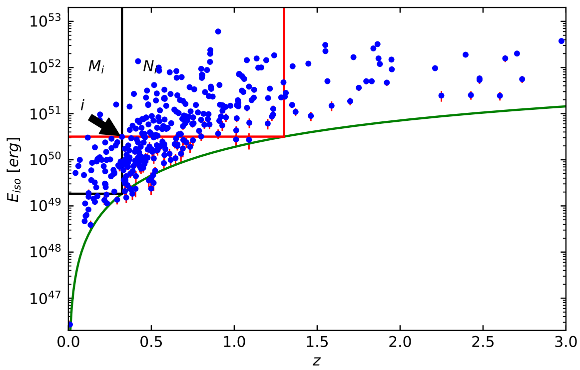

Fig. 3 Isotropic energy distribution of 334 Fermi sGRBs. The *blue dots* represent sGRBs and the *green line* is the fluence limit of 7×10^{-8} erg cm^{-2}.

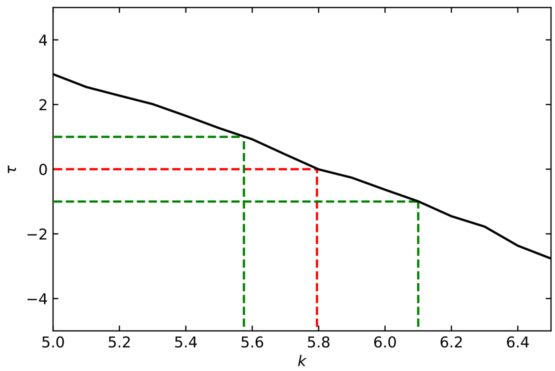

Fig. 4 The statistic τ as a function of the evolution parameter k. The best fitting $\tau = 0$ as well as 1σ error (i.e., $\tau = \pm 1$) corresponds $k = 5.79^{+0.31}_{-0.21}$. Thus, $g_k(z) = (1+z)^{5.79}$ is the best function to describe the isotropic energy evolution of sGRBs.

can see from Figure 2 that two distributions are similar. In order to further give a quantitative result, we perform the Kolmogorov-Smirnov test between the measured redshifts and the pseudo redshifts and obtain the p value is $P = 0.313$. This further confirms that our estimated redshift distribution is consistent with the observed one.

3 ISOTROPIC ENERGY FUNCTION AND FORMATION RATE

3.1 Lynden-Bell c^- Method

The Lynden-Bell c^- method is an effective non-parametric method for conducting the truncated data, which has been extensively used to analyze the luminosity/istropic energy and redshift distribution of the astronomical objects, such as quasars (see e.g., Lynden-Bell 1971; Efron & Petrosian 1992; Petrosian 1993), galaxies (see e.g., Kirshner et al. 1978; Loh & Spillar 1986; Peterson et al. 1986), and GRBs (see e.g., Lloyd-Ronning et al. 2002; Yonetoku et al. 2004, 2014; Wu et al. 2012; Yu et al. 2015; Pescalli et al. 2016; Zhang et al. 2018). In this work, we also use this method to study the isotropic energy function and formation rate of Fermi sGRBs.

The isotropic energy can be easily calculated with $E_{\rm iso} = 4\pi D_L^2(z) S_\gamma k_{\rm c}/(1+z)$, where S_γ represents the observed fluence, and $k_{\rm c}$ is the factor of the k-correction. If the isotropic energy and redshift of sGRBs are independent, the distribution of sGRBs can be simply written as $\Phi(E_{\rm iso}, z) = \rho(z)\phi(E_{iso})$, where $\phi(E_{\rm iso})$ is isotropic energy function, $\rho(z)$ is the sGRB formation rate at z. However, the isotropic energy exists a significant redshift evolution. Therefore, we need rewrite the isotropic energy function as $\Phi(E_{\rm iso}, z) = \rho(z)\phi(E_{\rm iso}/g_k(z))/g_k(z)$, where $\phi(E_{\rm iso}/g_k(\rm z))$ is the local (at $z = 0$) isotropic energy function, and $g_k(z)$ accounts for the evolution of $E_{\rm iso}$. Then, the isotropic energy at redshift $z = 0$ is $E_{\rm iso,0} = E_{\rm iso}/g_k(z)$, and $E_{\rm iso,0}$ is independent of z. The goal of our analysis is to obtain the local isotropic energy function $\phi(E_{\rm iso,0})$ and the formation rate $\rho(z)$.

Firstly, we need to remove the effect of the isotropic energy evolution and determine the value of k by assuming an evolution functional form of $g_{\rm k}(z) = (1+z)^k$ as done by many previous works (Lloyd-Ronning et al. 2002; Yonetoku et al. 2014; Yu et al. 2015; Zhang et al. 2018; Guo et al. 2020). Following Efron & Petrosian (1992), we use the non-parametric test method of a τ statistical method to derive the value of k.

In the $(E_{\rm iso}, z)$ plane as shown in Figure 3, for a random point of ith $(E_{\rm iso,i}, z_{\rm i})$, we can consider an associated set $J_{\rm i}$ as

$$J_{\rm i} = \{j | E_{\rm iso,j} \geq E_{\rm iso,i}, z_{\rm j} \leq z_{\rm i}^{\rm max}\}, \tag{7}$$

where $E_{\rm iso,i}$ is the isotropic energy of ith sGRB and $z_{\rm i}^{\rm max}$ is the maximum redshift at which the sGRBs with the isotropic energy $E_{\rm iso,i}$ can be detected by the Fermi detector. This range as a red rectangle region is shown in Figure 3. We define the number of sGRBs contained in this region as $N_{\rm i}$. In addition, we set a fluence limit of $S_{\gamma,\rm lim} = 7 \times 10^{-8}$ erg cm^{-2} to obtain as many data as possible as done by Yonetoku et al. (2014), Therefore, the isotropic energy limit at redshift z is given as $E_{\rm iso,lim} = 4\pi D_L^2(z) S_{\gamma,\rm lim}/(1+z)$. In Figure 3, there are 324 Fermi sGRBs above the fluence limit.

If $E_{\rm iso}$ and z are independent of each other, one would expect the number $R_{\rm i}$, $R_{\rm i} = Number\{j \in J_{\rm i} | z_{\rm j} \leq z_{\rm i}\}$, is uniformly distributed between 1 and $N_{\rm i}$. The test statistic τ is

$$\tau = \frac{\sum_i (R_{\rm i} - E_{\rm i})}{\sqrt{\sum_{\rm i} V_{\rm i}}}, \tag{8}$$

Table 2 Fermi sGRB Sample

GRB	z	$T_{90}^{\rm obs}$ (s)	$E_{\rm peak}^{\rm obs}$ (keV)	α	S_γ (10^{-6} erg cm^{-2})	$F_{\rm p}$ (10^{-6} erg cm^{-2} s^{-1})	$E_{\rm iso}$ (10^{50}erg)	$L_{\rm p}$ (10^{51} erg s^{-1})
GRB180715755	1.03	0.70 ± 0.29	902.28 ± 149.53	-0.11 ± 0.19	16.42 ± 1.10	3.34 ± 0.64	72.64 ± 4.88	29.97 ± 5.75
GRB180715741	0.576	1.66 ± 1.42	560.80 ± 89.15	-0.32 ± 0.14	20.82 ± 1.91	3.53 ± 0.68	21.34 ± 1.96	5.70 ± 1.10
GRB180703949	0.06	1.54 ± 0.09	136.88 ± 3.03	-0.77 ± 0.03	86.00 ± 1.21	18.27 ± 0.68	0.73 ± 0.01	0.17 ± 0.01
GRB180626392	0.454	0.96 ± 0.41	431.24 ± 81.89	-0.63 ± 0.20	5.61 ± 0.70	3.27 ± 0.60	3.28 ± 0.41	2.78 ± 0.51
GRB180625941	0.687	0.70 ± 0.68	576.02 ± 107.00	-0.17 ± 0.31	5.21 ± 0.61	2.74 ± 0.49	7.72 ± 0.90	6.84 ± 1.21
GRB180617872	0.301	1.92 ± 0.78	158.32 ± 17.95	-0.37 ± 0.20	3.30 ± 0.35	1.04 ± 0.19	0.76 ± 0.08	0.31 ± 0.06
GRB180602938	0.343	0.01 ± 0.74	384.51 ± 74.89	-0.60 ± 0.21	3.03 ± 0.38	4.41 ± 0.50	0.96 ± 0.12	1.88 ± 0.21
GRB180525151	1.311	0.54 ± 0.69	1011.93 ± 266.03	-0.49 ± 0.19	3.66 ± 0.36	2.91 ± 0.38	28.13 ± 2.76	51.54 ± 6.82
GRB180523782	2.395	1.98 ± 1.35	1434.52 ± 443.27	-0.35 ± 0.23	5.87 ± 0.66	2.63 ± 0.49	189.71 ± 21.39	288.52 ± 53.36
GRB180511437	0.213	1.98 ± 0.97	107.53 ± 11.92	-0.92 ± 0.15	6.12 ± 0.44	0.97 ± 0.25	0.73 ± 0.05	0.14 ± 0.04
GRB180511364	0.91	0.13 ± 1.21	744.00 ± 279.15	-0.83 ± 0.21	2.28 ± 0.32	2.81 ± 0.41	7.00 ± 0.98	16.43 ± 2.41
GRB180404848	0.098	0.54 ± 0.84	58.06 ± 6.25	-0.72 ± 0.34	1.88 ± 0.17	1.36 ± 0.18	0.05 ± 0.00	0.04 ± 0.01
GRB180402481	0.367	0.26 ± 0.18	335.38 ± 55.98	-0.13 ± 0.32	4.53 ± 0.60	2.99 ± 0.53	1.59 ± 0.21	1.43 ± 0.26
GRB180402406	0.808	0.45 ± 0.33	1326.79 ± 152.34	-0.37 ± 0.09	18.19 ± 0.80	10.21 ± 0.72	68.30 ± 2.99	69.30 ± 4.88
GRB180313978	0.277	0.08 ± 0.41	299.73 ± 40.45	-0.02 ± 0.24	2.62 ± 0.28	4.12 ± 0.44	0.50 ± 0.05	1.01 ± 0.11
...	...	...	...	...	...	...	...	...

The full table is available at *http://www.raa-journal.org/docs/Supp/ms4930Table2.pdf*.

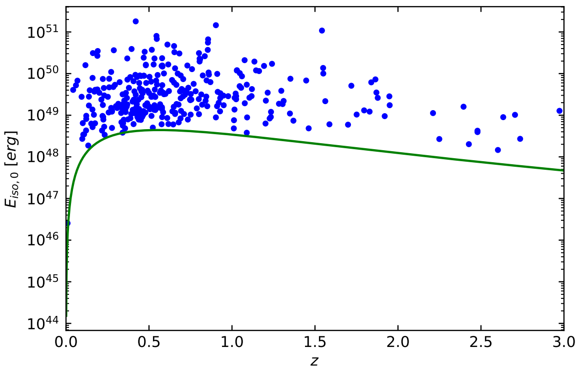

Fig. 5 Non-evolving isotropic energy $E_{\rm iso,0} = E_{\rm iso}/(1+z)^{5.79}$ of 324 Fermi sGRBs above the truncation line. The *green line* represents the fluence limit.

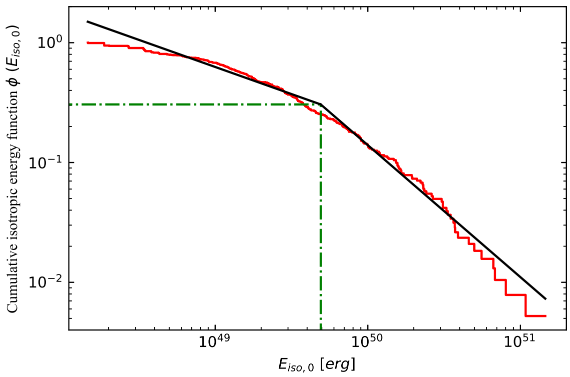

Fig. 6 Cumulative isotropic energy function of $\phi(E_{\rm iso,0})$, which is normalized to unity at the first point. The *black line* is the best fit with a broken power-law model. The isotropic energy function can be expressed as $\phi(E_{\rm iso,0}) \propto E_{\rm iso,0}^{-0.45\pm0.01}$ for dim sGRBs and $\phi(E_{\rm iso,0}) \propto E_{\rm iso,0}^{-1.11\pm0.01}$ for bright sGRBs, with a break energy of $E^b_{\rm iso,0} = 4.92 \times 10^{49}$ erg.

where $E_{\rm i} = (N_{\rm i}+1)/2$ and $V_{\rm i} = (N_{\rm i}^2 - 1)/12$ are the expected mean and the variance of $R_{\rm i}$, respectively. If $R_{\rm i}$ follows an ideal uniform distribution, then the samples of $R_{\rm i} \geq E_{\rm i}$ and $R_{\rm i} \leq E_{\rm i}$ should be equal, and the value of τ should be equal to zero. However, $E_{\rm iso}$ and z are not independent of each other. We change the value of k until the test statistic τ is zero. Figure 4 shows the value of the test statistic τ as a function of k. we find that the best fitting is $k = 5.79^{+0.31}_{-0.21}$. The distribution of non-evolving isotropic energy $E_{\rm iso,0}$ and z is shown in Figure 5.

3.2 Isotropic Energy Function

After remove the effect of the isotropic energy evolution, $E_{\rm iso,0} = E_{\rm iso}/(1+k)^{5.79}$, we can use the non-parametric method to derive the cumulative isotropic energy function ($\phi(E_{\rm iso,0})$) from the following equation

$$\phi(E_{\rm iso,0,i}) = \prod_{j<i}\left(1 + \frac{1}{N_{\rm j}}\right). \qquad (9)$$

Figure 6 shows the cumulative isotropic energy function. The shape of isotropic energy function roughly follows a broken power-law, and the best fitting is given by

$$\phi(E_{\rm iso,0}) \propto \begin{cases} E_{\rm iso,0}^{-0.45\pm0.01}, E_{\rm iso,0} < E^b_{\rm iso,0} \\ E_{\rm iso,0}^{-1.11\pm0.01}, E_{\rm iso,0} \geq E^b_{\rm iso,0} \end{cases} \qquad (10)$$

with the break energy $E^b_{\rm iso,0} = 4.92 \times 10^{49}$ erg. It is worth noting that the isotropic energy function here corresponds to $z = 0$, the isotropic energy function of sGRBs at redshift z is $\phi(E_{\rm iso,0})(1+z)^{5.79}$.

3.3 The Formation Rate

In order to get the formation rate of sGRBs, we define $J_{\rm i}'$

$$J_{\rm i}' = \{j | E_{\rm iso,o,j} \geq E^{lim}_{\rm iso,o,i}, z_{\rm j} \leq z_{\rm i}\}, \qquad (11)$$

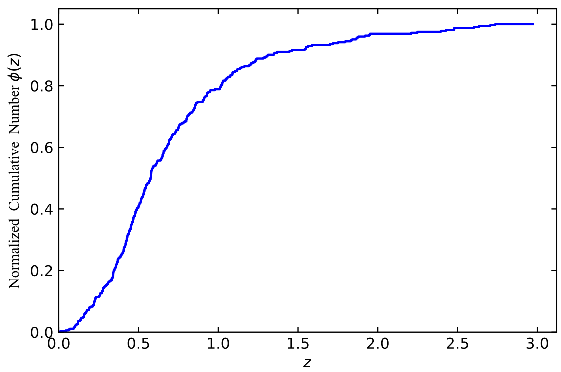

Fig. 7 Cumulative redshift distribution of sGRBs

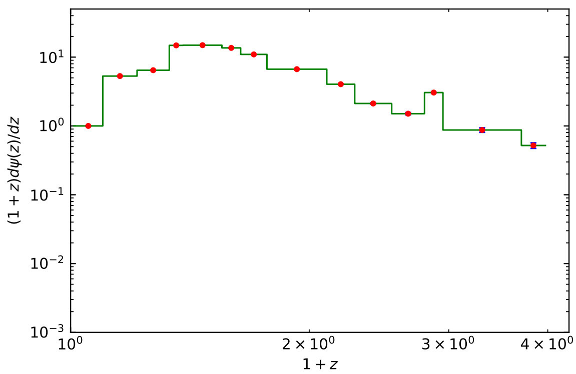

Fig. 8 Evolution of $(1+z)d\psi(z)/dz$ as a function of redshift z with 1σ errors, which is normalized to unity at the first point

where $z_{\rm i}$ is the redshift of ith sGRB, and $E^{lim}_{\rm iso,0,i}$ is the minimum isotropic energy, which can be observed at redshift $z_{\rm i}$. This range is the black rectangle region of Figure 3. The number of sGRBs in this region is $M_{\rm i}$. Similar to deriving the cumulative isotropic energy function, we can give the cumulative formation rate $\psi(z)$ as

$$\psi(z_{\rm i}) = \prod_{j<i}\left(1+\frac{1}{M_{\rm j}}\right), \tag{12}$$

and the result is shown in Figure 7.

The differential (not the cumulative) form of the sGRB formation rate is more useful for the purpose of comparison with the star formation rate. So we derive the differential formation rate of sGRBs with the following equation:

$$\rho(z) = \frac{d\psi(z)}{dz}(1+z)\left(\frac{dV(z)}{dz}\right)^{-1}, \tag{13}$$

where the factor $(1+z)$ represents the cosmological time dilation (Zhang et al. 2013), $\frac{dV(z)}{dz}$ is the differential comoving volume, which can be expressed as

$$\frac{dV(z)}{dz} = 4\pi\left(\frac{c}{H_0}\right)^3\left(\int_0^z \frac{dz}{\sqrt{1-\Omega_{\rm m}+\Omega_{\rm m}(1+z)^3}}\right)^2 \times \frac{1}{\sqrt{1-\Omega_{\rm m}+\Omega_{\rm m}(1+z)^3}}. \tag{14}$$

Figure 8 shows $(1+z)d\psi(z)/dz$ as a function of redshift z. From this figure, we can find that $(1+z)d\psi(z)/dz$ increases at $z<0.3$, remains constant for $z<0.3<0.7$, and then decrease at $z>0.7$. Figure 9 shows the formation rate of sGRBs. From this figure one can see that the formation rate $\rho(z)$ decreases at all redshift range, which is consistent with the result obtained in Zhang et al. (2018) and Guo et al. (2020), but it is different with the result of Yonetoku et al. (2014). We note that the result of Yonetoku et al. (2014) is similar to that in Figure 8. They might ignore the differential comoving volume $dV(z)/dz$ term as discussed in Yu et al. (2015). We use a broken power-law form to fit the formation rate, the best fitting is given by

$$\rho(z) \propto \begin{cases} (1+z)^{-4.02\pm1.34}, z<0.4 \\ (1+z)^{-4.93\pm0.30}, z\geq 0.4 \end{cases}. \tag{15}$$

According to Equation (15), we estimate the local sGRB formation rate is 17.43 ± 0.12 events Gpc^{-3} yr^{-1}. The previous resltus of Fong et al. (2015) that the local event rate is 10 events Gpc^{-3} yr^{-1}, and $\rho(0)=7.53$ events Gpc^{-3} yr^{-1} in Zhang et al. (2018), and $\rho(0)=15.5$ events Gpc^{-3} yr^{-1} in Guo et al. (2020) are consistent with our result.

In addition, using the $L_{\rm p}-z$ sample, we also analyze the luminosity function and the formation rate in the same way. We find that the best value of index k is $k = 6.43^{+0.24}_{-0.27}$, where the flux limit 5×10^{-7} erg cm^{-2} s^{-1} is adopted. After removing the effect

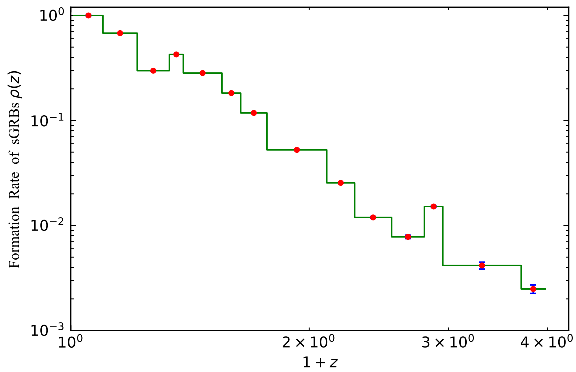

Fig. 9 Comoving formation rate of sGRBs, which is normalized to unity at the first point.

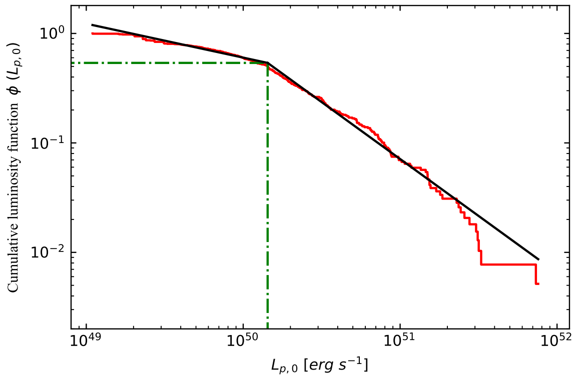

Fig. 10 Cumulative luminosity function of $\phi(L_{\rm p,0})$, which is normalized to unity at the first point. The luminosity function can be expressed as $\phi(L_{\rm p,0}) \propto L_{\rm p,0}^{-0.31\pm0.01}$ for $L_{\rm p,0} < L_{\rm p,0}^b$ and $\phi(L_{\rm p,0}) \propto L_{\rm p,0}^{-1.04\pm0.01}$ for $L_{\rm p,0} \geq L_{\rm p,0}^b$, where $L_{\rm p,0}^b = 1.43 \times 10^{50}$ erg^{-1} s^{-1}.

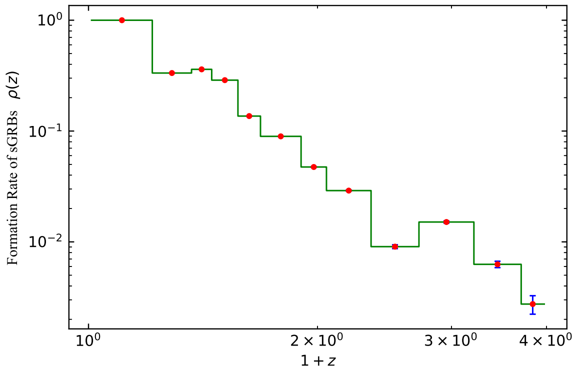

Fig. 11 Comoving sGRB formation rate of L_p sample, which is normalized to unity at the first point.

of the luminosity evolution, the corresponding cumulative luminosity function and the formation rate are reported in Figures 10 and 11. The luminosity function can also be well fitted with a broken power law. We obtain $\phi(L_{\rm p,0}) \propto L_{\rm p,0}^{-0.31\pm0.01}$ for $L_{\rm p,0} < L_{\rm p,0}^b$ and $\phi(L_{\rm p,0}) \propto L_{\rm p,0}^{-1.04\pm0.01}$ for $L_{\rm p,0} \geq L_{\rm p,0}^b$, where $L_{\rm p,0}^b = 1.43 \times 10^{50}$ erg^{-1} s^{-1}. Our results are well consistent with Zhang et al. (2018) and Guo et al. (2020). Nevertheless, our results are not sensitive to the limit of fluence and/or flux.

4 CONCLUSIONS AND DISCUSSION

Gamma-ray bursts are brief, intense, gamma-ray flashes in the universe, lasting from a few milliseconds to a few thousand seconds. For short gamma-ray bursts with duration less than 2 s, the isotropic energy, $E_{\rm iso}$, can be reliably measured than the luminosity, and the number density of bursts per $E_{\rm iso}$ interval may provide an independent or even more representative clue to the underlying physics of sGRBs.

In this work, we firstly use 22 sGRBs with known redshifts and well measured spectra to fit the $L_{\rm p} - E_{\rm p}$ correlation. Using this correlation, we derive the pseudo redshifts of 334 sGRBs observed by the Fermi detector. Then we for the first time construct the isotropic energy function and adopt it to estimate the sGRB formation rate. The fluence-truncation effect has been properly addressed by adopting a τ statistical method. We find that there exists a significant evolution of $E_{\rm iso}$, which is removed by $E_{\rm iso,0} = E_{\rm iso}/(1+z)^k$, where $k = 5.79^{+0.31}_{-0.21}$. After removing the redshift dependence, the isotropic energy function can be reasonably fitted by a broken power law. We obtain $\phi(E_{\rm iso,0}) \propto E_{\rm iso,0}^{-0.45\pm0.01}$ for dim segment, and $\phi(E_{\rm iso,0}) \propto E_{\rm iso,0}^{-1.11\pm0.01}$ for bright segment, where the break energy is $E_{\rm iso,0}^b = 4.92 \times 10^{49}$ erg (see Fig. 6). The shape of the isotropic energy function is similar to that of the luminosity function (see Fig. 9). Moreover, our power-law indices are comparable to those reported by Zhang et al. (2018) and Guo et al. (2020).

We find the sGRB formation rate is decreasing quickly, the best fit is $\rho(z) \propto (1+z)^{-3.18\pm1.02}$ for $z < 0.4$ and $\rho(z) \propto (1+z)^{-4.95\pm0.23}$ for $z \geq 0.4$, Zhang et al. (2018) and Guo et al. (2020) also obtained the similar results. We obtain the local formation rate of sGRBs is about 17.43 ± 0.12 events Gpc^{-3} yr^{-1}. It is believed that GRBs are originated from relativistic jets since breaks in the afterglow light curves are seen for many bursts. Although the jet breaks are rarely detected for sGRBs (Fong et al. 2015; Jin et al. 2018), we still need to account for the jet effect. Therefore, the observed sGRB formation rate can be corrected by the beam factor $f_{\rm B} = 1 - \cos(\theta_{\rm j})$, where $\theta_{\rm j}$ is the half-opening angle of the jet. Fong et al. (2015) reported the range of jet half-opening angles are from 6° to 26°. If we take this value and set the beaming factor as $f_{\rm B}^{-1} = 9 - 185$, the local event rate of sGRBs including the off-axis ones is $\rho_{0,\rm all} = 155.79 - 3202.35$ events Gpc^{-3} yr^{-1}.

Acknowledgements We acknowledge the use of public data from the Fermi catalogue. This work was supported in part by the National Natural Foundation of China (Grant No. 11763003), and by the Guangxi Natural Science Foundation (No. 2017GXNSFAA198094).

References

Abbott, B. P., Abbott, R., Abbott, T. D., et al. 2017, Phys. Rev. Lett., 119, 161101
Band, D., Matteson, J., Ford, L., et al. 1993, ApJ, 413, 281
Efron, B., & Petrosian, V. 1992, ApJ, 399, 345
Eichler, D., Livio, M., Piran, T., et al. 1989, Nature, 340, 126

Fong, W., Berger, E., Margutti, R., & Zauderer, B. A. 2015, ApJ, 815, 102
Ghirlanda, G., Ghisellini, G., & Firmani, C. 2006, New Journal of Physics, 8, 123
Goldstein, A., Veres, P., Burns, E., et al. 2017, ApJL, 848, L14
Guo, Q., Wei, D.-M., Wang, Y.-Z., et al. 2020, ApJ, 896, 83
Jin, Z.-P., Li, X., Wang, H., et al. 2018, ApJ, 857, 128
Kirshner, R. P., Oemler, A., J., & Schechter, P. L. 1978, 83, 1549
Kouveliotou, C., Meegan, C. A., Fishman, G. J., et al. 1993, ApJL, 413, L101
Lan, G. X., Zeng, H. D., Wei, J. J., & Wu, X. F. 2019, MNRAS, 488. 4607
Lipunov, V. M., Postnov, K. A., et al. 1995, ApJ, 454, 593
Lloyd-Ronning, Nicole M., Fryer, Chris L.& Ramirez-Ruiz, Enrico. 2002, ApJ, 574, 554
Loh, E. D., & Spillar, E. J. 1986, ApJL, 308, L1
Lynden-Bell, D. 1971, MNRAS, 155, 95
Mészáros, P. 2006, Reports on Progress in Physics, 69, 2259
Narayan, R., Paczynski, B., & Piran, T. 1992, ApJL, 395, L83
Pescalli, A., Ghirlanda, G., Salvaterra, R., et al. 2016, A&A, 587, A40
Peterson, B. A., Ellis, R. S., Efstathiou, G., et al. 1986, MNRAS, 221, 233
Petrosian, V. 1993, ApJL, 402, L33
Piran, T. 2004, Reviews of Modern Physics, 76, 1143
Sakamoto, T., Barthelmy, S. D., Barbier, L., et al. 2008, ApJS, 175, 179
Salvaterra, R., Guidorzi, C., Campana, S., Chincarini, G., & Tagliaferri, G. 2009, MNRAS, 396, 299
Salvaterra, R., Campana, S., Vergani, S. D., Covino, S., et al. 2012, ApJ, 749, 68
Wanderman, D., & Piran, T. 2010, MNRAS, 406, 1944
Wang, X.-G., Liang, E.-W., Li, L., et al. 2013, ApJ, 774, 132
Wang, F. Y., Dai, Z. G., & Liang, E. W. 2015, New Astron. Rev., 67, 1
Wu, S. W., Xu, D., Zhang, F. W., & Wei, D. M. 2012, MNRAS, 423, 2627
Yonetoku, D., Murakami, T., Nakamura, T., et al. 2004, ApJ, 609, 935
Yonetoku, D., Nakamura, T., Sawano, T., et al. 2014, ApJ, 789, 65
Yu, H., Wang, F. Y., Dai, Z. G., & Cheng, K. S. 2015, ApJS, 218, 13
Zhang, B. 2007, ChJAA (Chin. J. Astron. Astrophys.), 7, 1
Zhang, B. 2011, Comptes Rendus Physique, 12, 206
Zhang, F.-W., Fan, Y.-Z., Shao, L., et al. 2013, ApJL, 778, L11
Zhang, G. Q., & Wang, F. Y. 2018, ApJ, 852, 1